

Experimental investigation on ferrofluid properties of Cd doped Co-Zn ferrites

R. Manimegalai^{a,*}, S. Sendhilmathan^b, V. Chithambaram^c

^aDepartment of Physics, K.Ramakrishnan College of Engineering Trichy-621112, Tamil Nādu, India,

^bDepartment of Physics, University College of Engineering, Pattukkottai Campus, Rajamadam-614701.Tamilnadu, India.

^cDepartment of Physics, PERI Institute of Technology, Mannivakkam, Chennai – 600048

Cadmium substituted Co-Zn ferrites $Co_{0.5}Zn_{0.5}Cd_xFe_{(2-x)}O_4$ ($x=0.0, 0.1, 0.2, 0.4,$ and 0.5) were fabricated by using the Co-precipitation method. The molecular composition and prepared samples of cubic spinel structures was characterized using X-ray diffraction peak (XRD). X-ray diffraction patterns obtained the most intensive peak at (311) crystallographic planes for $x=0.5$. Williamson-Hall (W-H) relation was associated with XRD data to determine the crystallite sizes range from 25.356 nm to 35.632 nm and strain value brought into being 0.0024 to 0.0021. Tetrahedral and octahedral sites of hopping length were found to diminish from 3.6707Å-3.6332Å and 2.9967Å-2.9662Å respectively due to the addition of Cd ion concentration. TEM analysis reveals the presence of spherical shape nanoparticles with agglomeration for the prepared samples. It could be referenced based on the investigation of results for molecule size by two XRD and TEM strategies which demonstrate the development of nanomaterials and doping of cobalt ferrites. TEM results are well agreed with the XRD diffraction pattern in crystallite size by using Scherrer's formula. Fourier Transform Infrared Spectroscopy (FTIR) spectra analysis were carried out on synthesized ferrite samples and observed ν_1 and ν_2 strong absorption band in the range 400-4000 cm^{-1} be the possession to tetrahedral (A) and octahedral (B) sites. In FTIR, the increase of Cd^{2+} ion in Co-Zn ferrites leads to diminishing peak values towards lower wavenumbers. It is feasible to tune the magnetic characteristics of cobalt ferrite as a potential material for diverse technological applications by substituting Zn^{2+} and Cd^{2+} for cobalt magnetic ions.

(Received January 28, 2022; Accepted June 2, 2022)

Keywords: Cobalt ferrite, cadmium doping, Crystalline size, Williamson-Hall method, Tetrahedral, Octahedral

1. Introduction

Magnetic nanoparticles are considered by experts in various fields because they are used in a data structure, clinical diagnosis, Ferrofluid productions, and so on. Recent researches of the utilization of magnetic nanoparticles have been tremendously expanded in biomedical applications. Numerous scientists have been centered around the improvement of attractive nanoparticles (MNPs) just as to work on their relevance in various regions. Current researchers mainly concentrated on nanoparticles due to their excellent magnetic and electric properties [1]. Magnetic Hyperthermia, bioimaging, Magnetic Resonance Imaging (MRI), and drug delivery applications are characterized based on the following spinel ferrites magnetic properties such as spin-glass-like behavior, spin canting effect and superparamagnetism high electrical resistivity, and high permeability [2, 3]. Spinel ferrites have excellent magnetic properties, structural and electrical properties compared to various magnetic nanoparticles [5]. Since, nano synthesized spinel ferrites (MFe_2O_4 , $M = Zn, Co, Mn, Ni, Cu,$ etc. general formula of ferrites) has been used to implement in hyperthermia-based magnetic proficiency, electronic devices, sensors, and energy storage device [6-7]. Conversely, these properties differ due to the range and profile of the mixture of nanoparticles based on the synthesis process. In this way, fitting these boundaries can empower us

* Corresponding authors: manimegalaiarthiban@gmail.com
<https://doi.org/10.15251/DJNB.2022.172.661>

to manage the properties of the nanosized ferrites and render them appropriate for different innovative applications.

The nano synthesized $\text{Co}_{1-x}\text{Zn}_x\text{Fe}_2\text{O}_4$ ferrites are fully concentrated until now due to their exceptionally attractive, electrical, and photosynthetic properties [8]. The hyperfine parameters of the $\text{Co}_{0.3}\text{Zn}_{0.7}\text{Fe}_2\text{O}_4$ nanoscale were achieved at 16.6nm using the parallel precipitation method via the ball milling process [9]. The normal spinel ferrofluid of the entire ZnFe_2O_4 is toxic and soft-magnetic while using CoFe_2O_4 is toxic and hard magnetic reverse spinel. Similarly, $\text{Ni}_{0.3}\text{Zn}_{0.7}\text{Fe}_2\text{O}_4$ nanoparticles were prepared with PVA coated by using sol-gel auto-combustion fabrication techniques, and the estimated magnetization and crystal size is 16-19 emu/g [10]. The nanoparticles are coated with CoFe_2O_4 oleic acid-coated water-dispersible, which is covalent by heat transfer, improving the colloidal consistency and biomedical application [11]. The addition of CoFe_2O_4 with Zn leads to an increase in particle size of 45 to 49 nm using a sol-gel automatic combustion method [12]. Due to high moderate saturation magnetization, large magneto strictive coefficient, and high coercivity, the cobalt ferrite is considered an important magnetic metal oxide among the various types of spinel ferrites. The CoFe_2O_4 has an inverse spinel structure yet when divalent metal particles such as Zn, Cd, Ni, and so forth are drugged in cobalt ferrite; it changes the construction of cobalt ferrite from converse spinel to ordinary spinel ferrites [13].

Generally, cobalt and zinc ferrites consist of hard and soft magnetic materials respectively, but the addition of Zn^{2+} leads to reduce the hardness of cobalt ferrites. Zinc is one of the most effective soft magnetic materials in various alternatives and has good chemical stability, high sensitivity to temperature, and high coercivity properties[14]. Cobalt ferrite ferromagnetic of high concentration and coercivity magnetic properties is converted from a magnetic field to a super magnetic field when converting non-magnetic zinc [15]. Superparamagnetic properties are widely discussed in biomedical applications.

Khedri et al [16] examined the cubic structure of $\text{M}_{0.3}\text{Cu}_{0.2}\text{Zn}_{0.5}\text{Fe}_2\text{O}_4$ ferrites and also observed the nonporous sponge by using FE-SEM and TEM analysis. As final results, Neel type structure exists in Co-Zn ($x=0.3$) ferrofluid samples. To synthesize the Co-Zn ferrites and to maintain the magnetic particles without compromising their properties by replacing Co^{2+} and Zn^{2+} particles, which prompts the advancement of different diverse magnetic attributable to variety in sublattice trade connections inside the spinel cross-section[8,25].

Tatarchuk et al [19] reported the spinel lattice correlation among the sites A and B (Tetrahedral and octahedral) when the doping material non-magnetic Zn^{2+} leads to an increase in the value of saturation magnetization in nanosized CoFe_2O_4 at a ratio of $X=0.5$, due to inter-sublattice A-O-B (J_{AB}). Over this proportion ($X < 0.5$), polarization begins to diminish because of the development of Fe^{3+} particles from [B] site to (A) site in place of Zn^{2+} particles which especially involve (A) site when $X > 0.5$. As concluded from several pieces of research that magnetization of $\text{Co}_{1-x}\text{Zn}_x\text{Fe}_2\text{O}_4$ increases dramatically when limiting $0.1 \leq X \leq 0.5$ [30]. The above $X=0.5$ non-magnetic iron's tendency to formulate octahedral site, that result was strengthening the short-range interaction B-O-B (J_{BB}) and weakening the long-range interactions A-O-A (J_{AA}) consequently. Therefore, the range $X > 0.5$ of magnetic properties of $\text{Co}_{0.5}\text{Zn}_{0.5}\text{Fe}_2\text{O}_4$ investigation plays a promising role in nanoparticle research.

However, based on previous research so far, the structure in $\text{Co}_{1-x}\text{Zn}_x\text{Fe}_2\text{O}_4$ continues to test the full intensity to determine the properties of the magnetic and dielectric properties of ferrite. Many kinds of research do not fully discuss the properties of a particular system of $\text{Co}_{1-x}\text{Zn}_x\text{Fe}_2\text{O}_4$ ferrite structures, some of which have appeared with excellent results while concentrated in Co series. An increase of soft and hard metallic materials the following properties such as mixed magnetic phase, non-collinear spinel structure, and superparamagnetic clusters have been recognized in the ferrites [21], especially $\text{Co}_{0.5}\text{Zn}_{0.5}\text{Fe}_2\text{O}_4$ as drawn in unique consideration. The semi-soft magnetic CoFe_2O_4 were studied by using the sol-gel method. These experimental results show dielectric constants made nanoparticles are a significant member in high-frequency magnetic devices [26].

The hybridization technique of nano synthesis spinel ferrites is of particular importance informative of their uniqueness and competency in modern applications [22-23]. Among the synthesis procedures co-precipitation method has an efficient synthesis technique due to low cost, sensible preparation time, and well-known large production of nano ferrites which is industrially

important [24]. Be that as it may, these nanometric ferrites are powerless against a decrease of magnetization and attractive requesting temperature because of the unwanted impacts of surface twist inclining and superparamagnetism identified with limited size impact [27]. Using heat treatment can increase and prevent the temperature of the ferrites, but the disadvantage is that it increases the particle size. Synthesis of the chemical coprecipitation method of nanoferrites following the mechanical ball milling process seems to be an appropriate technique for achieving high magnetic quality nanoparticle spinel ferrites without compromising their industrial requirements. The coprecipitation method produces a uniform powder with a maximum limit and does not use any organic fuels.

In this regard, we have prepared $Co_{0.5}Zn_{0.5}Cd_xFe_{(2-x)}O_4$ ferrite nanoparticles were synthesized by using the chemical co-precipitation method commencing with aqueous salt solutions. Hence, the present investigation examined the synthesis, structural changes, and Mechanical properties of $Co_{0.5}Zn_{0.5}Cd_xFe_{(2-x)}O_4$ ferrites. The structures were characterized by X-ray diffraction (XRD) and the sizes of the magnetic nanoparticles were determined by using Transmission Electron Microscope (TEM). Furthermore, the thermal of ferrites were investigated by using TG-DTA analysis. FTIR studies were conducted on the prepared samples at the wavelength number 400^{-1} - $4000cm^{-1}$. W-H method was performed to evaluate the crystallite size from the XRD peaks by using Scherer's formula.

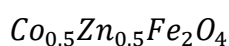
2. Experiments and methods

Co-precipitation method was performed to synthesis the Co-Zn with Cd doped $Co_{0.5}Zn_{0.5}Cd_xFe_{(2-x)}O_4$ magnetic nanoparticles. It is a common method most widely for the synthesis of ferrofluid interacted with fluid-based magnetic nanoparticles provide an efficient magnetic property. Based on the aqueous solution and surfactant was used to fabricate the spinel ferrite nanoparticles [33]. Then, at that point, the arrangement is exposed to various techniques like decantation, magnetic detachment, centrifugation, and weakening. To eliminate the agglomeration of attractive nanoparticles, this arrangement is usually covered with a shell of the right material. Afterward, the arrangement is subjected to various techniques to remove the agglomerations of attractive nanoparticles.

2.1. Synthesis of ferrofluids

The ferrite nanoparticles $Co_{0.5}Zn_{0.5}Cd_xFe_{(2-x)}O_4$ ($x=0.0, 0.1, 0.2, 0.4, \text{ and } 0.5$) with different proportions of the mix were synthesized by using the co-precipitation method. The parent material grades $Co(NO_3)_2 \cdot 6H_2O$, $Zn(NO_3)_2 \cdot 6H_2O$, and $Fe(NO_3)_3 \cdot 9H_2O$ and $Cd(NO_3)_2 \cdot 4H_2O$ respectively, which are extracted from a proper stoichiometric ratio and constant stirring in 100 ml distilled water with 30 M NH_4OH solution. The Table 1 shows the effect of concentrations on Co-Zn ferrofluids. The surfactants are used to stabilize the magnetic nanoparticles. Oleic acid is normally utilized as a surfactant, which frames the goodwaterproofing shell around the attractive magnetic nanoparticles. In the production of ferrofluid, nanoparticles with acetic acid mixing states are important because it is used to avoid the agglomeration of nanoparticles.

Magnetic nanoparticles were fabricated with different proportions of nominal values with aqueous solutions in their respective stoichiometric at $80^{\circ}C$. The blended arrangement was added to the arrangement of NH_4OH drop-wise under consistent mixing and afterward the precipitation happened promptly to change the response for a dark shading (brown), normal for this ferrite. The reaction temperature was maintained at $80^{\circ}C$ for 2-3 hours and cooled in precipitate when the precipitate reaches the liquid state. The pH arrangement was maintained at a constant temperature when NH_4OH was added to the precipitation of ferrous fluids with magnetic nanoparticles. By stirring the reactants, the de-ionized water produces a reduction in the reaction's PH value from 12 to 7. This led to the development of a copper-based metal hydroxide under temperature conditions. Fig 1 illustrated the $Co_{0.5}Zn_{0.5}Cd_xFe_{(2-x)}O_4$ ($x=0.0, 0.1, 0.2, 0.4, \text{ and } 0.5$) synthesis process by Co-precipitation method.



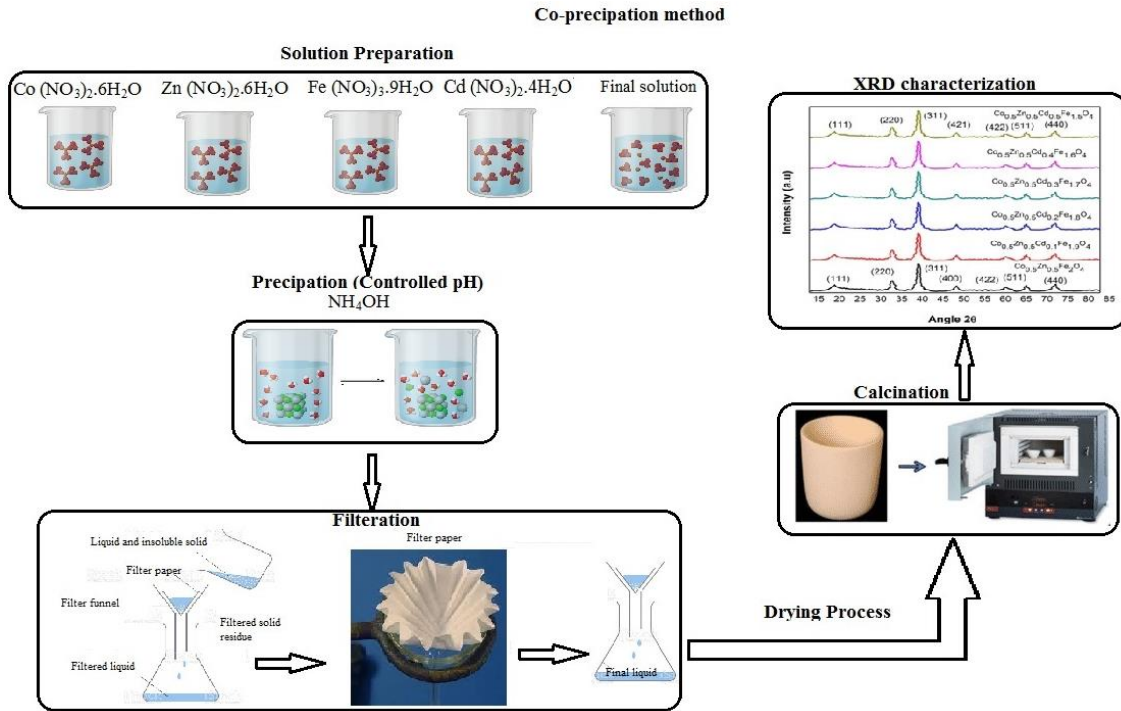
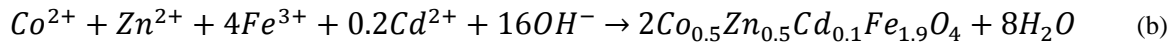
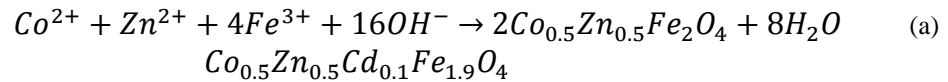


Fig.1. Co-precipitation synthesis method.

Table 1. Nominal values of Cd substituted $\text{Co}_{0.5}\text{Zn}_{0.5}\text{Cd}_x\text{Fe}_{(2-x)}\text{O}_4$ magnetic Nanoparticles.

Samples	Concentration mol/l			
	Co	Zn	Cd	Fe
$\text{Co}_{0.5}\text{Zn}_{0.5}\text{Fe}_2\text{O}_4$	0.1	0.1	-	0.4
$\text{Co}_{0.5}\text{Zn}_{0.5}\text{Cd}_{0.1}\text{Fe}_{1.9}\text{O}_4$	0.1	0.1	0.38	0.02
$\text{Co}_{0.5}\text{Zn}_{0.5}\text{Cd}_{0.2}\text{Fe}_{1.8}\text{O}_4$	0.1	0.1	0.36	0.04
$\text{Co}_{0.5}\text{Zn}_{0.5}\text{Cd}_{0.3}\text{Fe}_{1.7}\text{O}_4$	0.1	0.1	0.06	0.04
$\text{Co}_{0.5}\text{Zn}_{0.5}\text{Cd}_{0.4}\text{Fe}_{1.6}\text{O}_4$	0.1	0.1	0.08	0.32
$\text{Co}_{0.5}\text{Zn}_{0.5}\text{Cd}_{0.5}\text{Fe}_{1.5}\text{O}_4$	0.1	0.1	0.1	0.3

The particle conglomerates are easily formed during the synthesis of Co-Zn ferrofluid Magnetic nanoparticles. The problem was avoided by applying 5 ml of oleic acid as a surfactant and outer layer material and stirring well for 2 h at 80°C . The solution is completely ionized when the pH value decreases from 12-7 due to the addition of oleic acid. Therefore, it inhibits the accumulation of particles by enhancing electrostatic dissociation and binds the carboxylate groups to the ferrite surface to retain the ferrofluid. To obtain the particles free of salt and chlorine compounds was washed twice in 100 ml distilled and deionized water with ethanol and acetone to eliminate surplus chemical agents commencing the solution. Surfactant fluid such as ethanol, acetone, and water contents are segregated and water the measuring goblet content was then separated for 20 min at 4000 RPM. It was dried at a temperature of 90°C for 20 h and established as the best powder granules for XRD and FTIR analysis.

3. Materials characterization

Co-Zn with cadmium ($x=0.0-0.5$) doped ferrofluid was successfully prepared by magnetic nanoparticles using a co-precipitation method. Thermal properties of the magnetic materials and functions of temperature were determined by TG-DTA under the nitrogen atmospheric condition with the temperature range varying from 23°C to 1200°C . X-ray diffraction pattern analysis were carried out for all prepared samples of crystal structures of $\text{Co}_{1-x}\text{Zn}_x\text{Fe}_2\text{O}_4$ magnetic nanoparticles and it was recorded in 2θ scale of 20° , and 80° by Rigaku X-ray diffractometer having Cu K α radiation ($\lambda=1.78899\text{\AA}$, 30kV and 16 mA). The presence of radiation at the room temperature is 15° to 95° with a corresponding scanning speed of $0.002^{\circ}\text{S}^{-1}$, incidence angle 5° and step time 0.2s. The International Center for Diffraction Data was used to evaluate and examine the X-ray diffraction pattern (ICDD-PDF2) information base and the WINJADE 8.5 programming for distinguishing proof and contrasted to CoFe_2O_4 quality. FTIR spectra data was noticed for the preserved samples of ferrites in a wave range of 400 cm^{-1} – 4000 cm^{-1} (resolution is 4 cm^{-1}) by using Shimadzu 8400 spectrophotometer. Spectra data were recorded based on the transmittance method and the dried samples were located on a silicon substrate exposed to infrared radiation.

4. Results and discussion

4.1. XRD analysis and particle characterization

Fig2 exhibit the XRD spectra of Cd^{2+} doped $\text{Co}_{0.5}\text{Zn}_{0.5}\text{Cd}_x\text{Fe}_{(2-x)}\text{O}_4$ ($x=0.0, 0.1, 0.2, 0.3, 0.4, \text{ and } 0.5$) ferrite nanoparticles. As a resultant, different diffraction peak intensities at 2θ values are indexed from the corresponding (111), (220), (311), (400), (422), (440), and (511) crystal planes. The high-intensity peaks were observed for 311 crystal planes, which represents strong reflection due to increasing Cd^{2+} iron concentrations and improved characteristics of spinel structure of Co-Zn ferrite. The peak broadenings are showing that the nanocrystalline phase formation. However, the diffraction intensity of all the individual peaks has increased in XRD patterns when increasing Cd^{2+} ions Co-Zn ferrites while compared to the peaks of $\text{Co}_{0.5}\text{Zn}_{0.5}\text{Fe}_2\text{O}_4$ Ferrites samples. In this all cases of peak broadening values are good agreed with the JCPDS 22-1086 powder diffraction data file. The higher peak intensities of crystal size are calculated by using the Debye Scherrer formula [29].

$$D = \frac{0.9\lambda}{\beta \cos\theta} \quad (1)$$

where $\lambda=1.543\text{ nm}$, β -full width at half maxima (FWHM) of XRD peaks, θ -Bragg's angle and D-particle size respectively. The lattice constant (a) is calculated by using the following mathematical equation as

$$\frac{1}{d^2} = \frac{h^2 + k^2 + l^2}{a^2} \quad (2)$$

where d is an Interplanar spacing, h, k and l are miller indices. All the cases of calculated lattice constant and crystal sizes, X-ray density, bulk density and porosity estimated values are displayed in Table 2. As clearly shows the increases of lattice constant (8.37 \AA - 8.54 \AA) and crystal size which ensure the effect of Zn^{2+} and Cd^{2+} iron-strong presence in prepared ferrite samples. Due to larger ionic radii of Cd^{2+} (1.12 \AA) as compared to Co (0.82 \AA), Zn (0.87 \AA) and Fe^{+2} (0.76 \AA). The dimension of the unit cell is slightly changed as a resulting change in lattice parameters due to shrinkage by partial replacement of Fe^{2+} and Cd^{2+} ions. This may be substitution of Cd and Fe in the prepared ferrite structures causes the Zn ions to commence to engage in the sites of Fe establish in the tetrahedral sites and also displacing of Co ions causes the Fe ions to migrate and increases octahedral sites. Therefore, the entire inverse spinel structure is converted into a normal spinel structure. These processes ensure the highest peak in the X-ray diffraction patterns were observed from the prepared samples. These processes ensure that the high peak intensities in

the X-ray diffraction patterns in our prepared samples. As the concentration of Cd atoms increases $Co_{0.5}Zn_{0.5}Cd_xFe_{(2-x)}O_4$ Magnetic nanoparticles are ensured that in the normal spinel structure of ferrites [30].

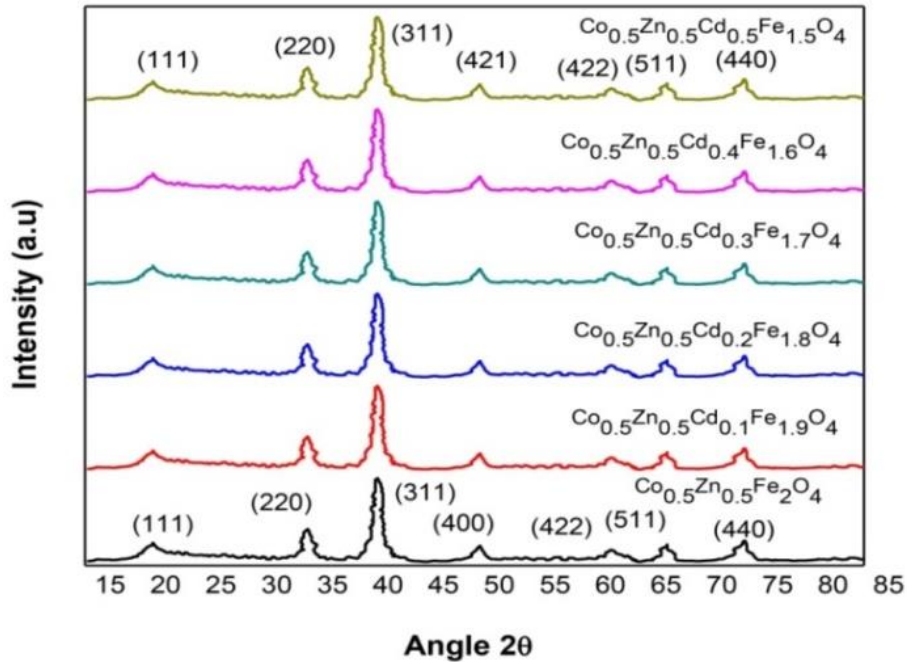


Fig.2.XRD diffraction patterns of $Co_{0.5}Zn_{0.5}Cd_xFe_{(2-x)}O_4$ (0.0, 0.1, 0.2, 0.3, 0.4 and 0.5).

Table 2. Variation of lattice constant 'a', crystallite size 'D', x-ray density ' d_{x-ray} ', bulk Density percentage porosity (P %).

Sample	Lattice constant	Crystallite Size	W-H	TEM	X-ray density	Bulk Density	Porosity
	a (Å)	D(nm)	D(nm)	D(nm)	(g/cm ³)	(g/cm ³)	P (%)
$Co_{0.5}Zn_{0.5}Fe_2O_4$	8.4772	25.35	17.25	24.56	5.185	9.103	82.4
$Co_{0.5}Zn_{0.5}Cd_{0.1}Fe_{1.9}O_4$	8.4537	27.87	24.93	26.52	5.354	8.856	72.5
$Co_{0.5}Zn_{0.5}Cd_{0.2}Fe_{1.8}O_4$	8.4305	30.45	32.93	31.46	5.523	8.652	65.7
$Co_{0.5}Zn_{0.5}Cd_{0.3}Fe_{1.7}O_4$	8.4284	32.81	34.92	32.45	5.638	8.457	62.3
$Co_{0.5}Zn_{0.5}Cd_{0.4}Fe_{1.6}O_4$	8.4118	33.88	28.06	31.56	5.813	8.323	58.4
$Co_{0.5}Zn_{0.5}Cd_{0.5}Fe_{1.5}O_4$	8.3909	35.63	34.6	33.78	5.984	8.211	55.3

X-ray density

$$\Delta x_{Ferrite} = \frac{8M}{Na^3} = \frac{8 * \text{Molecular weight of the sample}}{\text{Avogadro's number} * \text{Lattice constant}} \quad (3)$$

Bulk density formula expressed as follows

$$d_{bulk} = \frac{\text{Mass}}{\text{Volume}} \quad (4)$$

The porosity was estimated using the following expression

$$Porosity = \left(1 - \frac{d_{exp}}{d_{theoretical}}\right) X100 \quad (5)$$

The X-ray density, ionic radii, anions bonding strength by hoping length of A and B sites, stacking fault coefficients, and micro strains were estimated by using the above equations from (1)-(5) and presented in Table 3 and 4.

$$L_A = \frac{a \times \sqrt{3}}{4} \quad (6)$$

$$L_B = \frac{a \times \sqrt{2}}{4} \quad (7)$$

where L_A -Hoping length as the distance between the magnetic ions in tetrahedral sites and L_B -Hoping length is the distance between the magnetic ions in octahedral sites.

$$A - O = \left(u - \frac{1}{4}\right) a\sqrt{3} \quad (8)$$

$$B - O = \left(\frac{5}{8} - u\right) a \quad (9)$$

In Co-Zn ferrites, oxygen value u is 0.382, and A-O and B-O represent the Bonding length between A ion and oxygen respectively [31].

$$r_A = \left(u - \frac{1}{4}\right) a\sqrt{3} - r(O^{2-}) \quad (10)$$

$$r_B = \left(\frac{5}{8} - u\right) a - r(O^{2-}) \quad (11)$$

where r_A and r_B are ionic radius for A site and B-site respectively, $r(O^{2-})$ the ionic radius of oxygen ion (1.35Å).

$$\alpha = \left[\frac{2\pi^2}{45\sqrt{3}} \right] \frac{[\Delta 2\theta]}{\tan\theta_{hkl}} \quad (12)$$

α -Stacking fault coefficient, $\Delta 2\theta$ -Standard and observed 2θ values

$$micro - strain (\epsilon) = \frac{\beta \cos\theta}{4} \quad (13)$$

$$Dislocation's density \rho_D = \frac{1}{D^2} \quad (14)$$

Table 3. Hopping lengths 'LA and LB', strain 'ε', dislocation density 'η' with cadmium ion concentration.

Cobalt Ion concentration (x)	Hopping length		Strain ε	Dislocations Density η(Å ⁻²)
	L _A (Å)	L _B (Å)		
0	3.6707	2.9967	0.002145	0.0015
0.1	3.6605	2.9884	0.001874	0.0012
0.2	3.6505	2.9802	0.001429	0.00092
0.3	3.6496	2.9794	0.002276	0.00097
0.4	3.6424	2.9736	0.002427	0.00087
0.5	3.6332	2.9662	0.001822	0.00074

Table 4. Bonding length, Ionic Radii, and stacking fault coefficient.

Cobalt Ion concentration (x)	Bonding length		Ionic Radii $r_A(\text{Å})$	Ionic Radii $r_B(\text{Å})$	Stacking fault coefficient
	A-O (Å)	B-O (Å)			
0	1.9380	2.0599	0.5880	0.7099	0.00343
0.1	1.9327	2.0542	0.5827	0.7042	0.00378
0.2	1.9274	2.0486	0.5774	0.6986	0.00394
0.3	1.9269	2.0481	0.5769	0.6981	0.00404
0.4	1.9231	2.0440	0.5731	0.6940	0.00421
0.5	1.9183	2.0389	0.5683	0.6889	0.00457

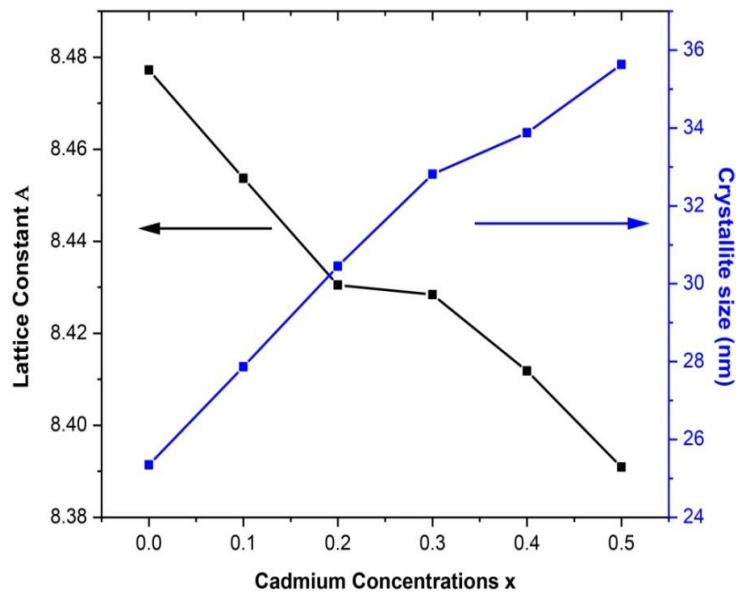


Fig.3. Lattice parameter and crystal size as functions of Cd concentration.

Fig3 shows the crystallite size and lattice parameter which extracted from the XRD diffraction patterns by increasing Cd ion concentrations. An increment of the $Co_{0.5}Zn_{0.5}Cd_xFe_{(2-x)}O_4$ (x=0.0, 0.1, 0.2, 0.3, 0.4 and 0.5) lattice parameter was seen with the consideration of cadmium; the cross-section boundary of $CoZnCdFe_2O_4$ is (0.838 nm), true to form because the nuclear span for Zn is bigger than the Cd atomic radius. The increases in crystallite size as a function of Cd ions concentration clearly explain the relationship between the parameters in a linear manner. However, the crystallite size increases with the increases of Cd ion concentrations in Co-Zn ferrites as seen in Fig3.

4.2. Williamson-Hall (W-H)

The Williamson-Hall (W-H) method to the relation with crystal size is given by

$$\beta \cos \theta = \frac{K\lambda}{D} + 4\epsilon \sin \theta$$

where $K=0.9$ homogenous crystal size, λ -Wavelength of X-ray, θ -Bragg's angle, ϵ - Strain distribution, D -average crystal size.

The Williamson-Hall (W-H) method as compared to Debye -Scherrer formula is one of the best methods for explaining the strain behavior in prepared magnetic samples as shown. In the case of a lower strain, $\epsilon=0$ of the Williamson-Hall (W-H) method is diminished Debye -Scherrer

equation. Fig4 shows the crystal size and strain value shape of the interference of the Y-axis and the slope of the lines as determined from the W-H method and which are presented in Tables3 and 4. Similarly, Fig 5 shows the strain plots with the corresponding relation between normal fit and linear fit values. The crystal size and strain have been found to range from 17 nm to 34.6 and 0.00247 -0.00212, by W-H plot respectively. It is noticed that strain decreased gradually on XRD peaks with negligible effects. As a result of cadmium addition in cobalt, ferrite leads to decreases than for Zn ions due to compressive strain.

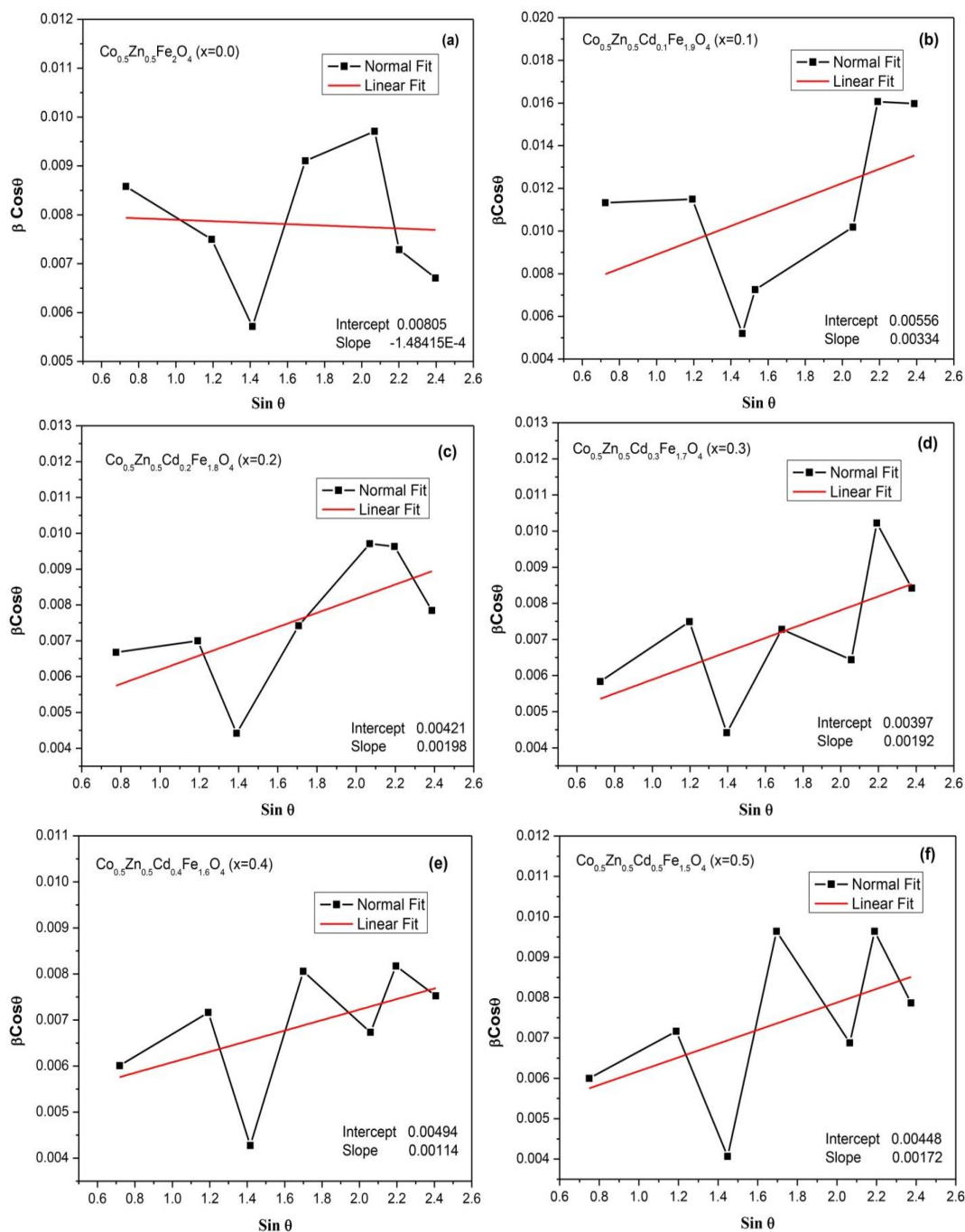


Fig.4. Cadmium doped Co-Zn ferrites Williamson-Hall plot.

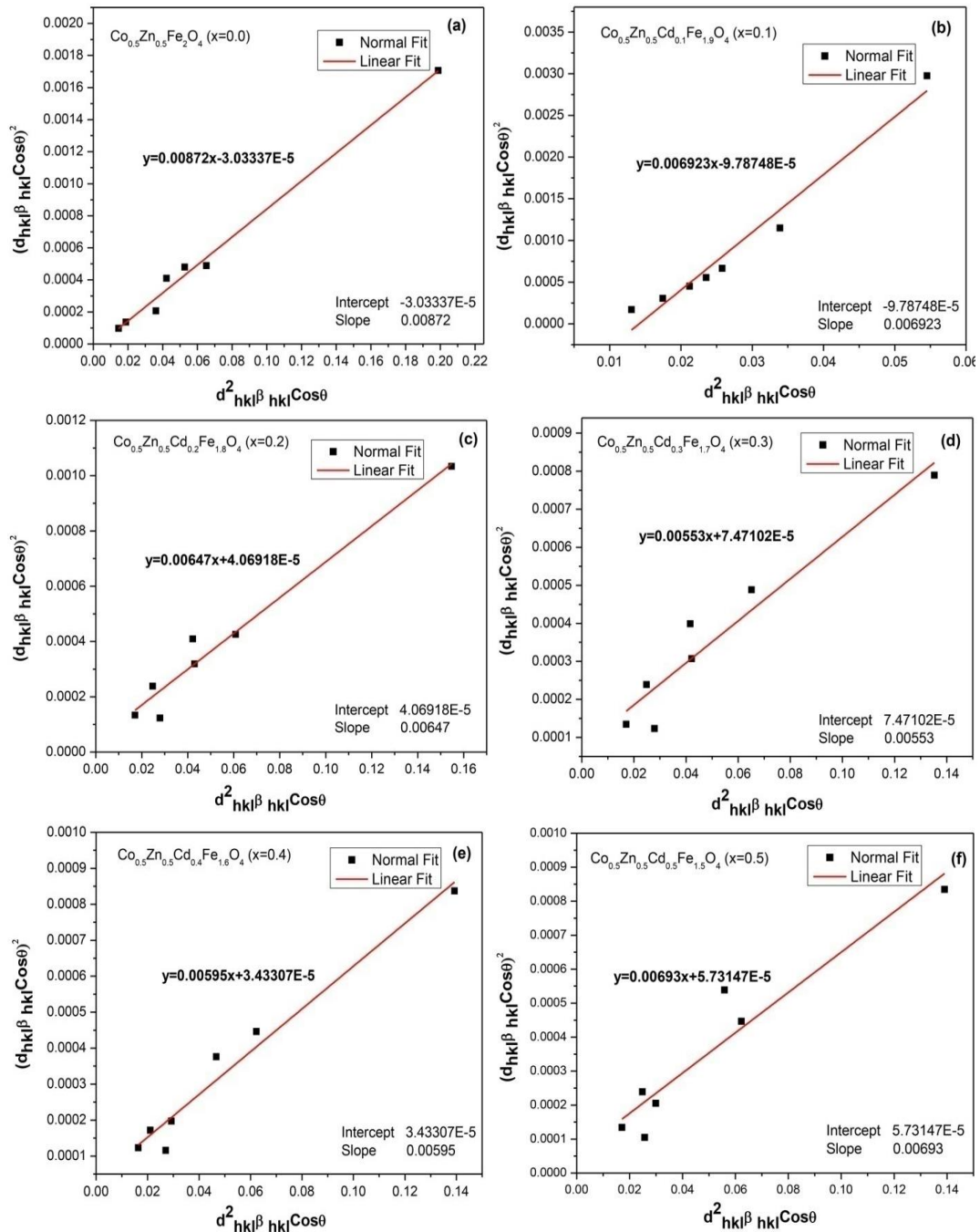


Fig.5. Cadmium doped Co-Zn ferrites strain plots.

4.3. FTIR spectral measurements

Fig6 shows the Fourier transform infrared spectroscopy (FTIR) graphical representation all prepared samples were observed in the wave range from 4000 cm^{-1} to 400 cm^{-1} . The FTIR study reveals the distribution of cations between Co-Zn octahedral and tetrahedral sites by the addition of Cd ferrites. Due to interatomic vibration, the existence band was received from the spectra. The spectra range from 400 cm^{-1} to -4000 cm^{-1} ensure that the spinel structure of Co-Zn ferrites with Cd^{2+} and Fe ion-doped samples.

The FTIR spectra exhibit two high significant bands between 580 cm^{-1} - 620 cm^{-1} having a place with the extending vibration modes related to the metal-oxygen absorption groups Fe-O bonds in the crystalline size of $\text{Co}_{0.5}\text{Zn}_{0.5}\text{Cd}_x\text{Fe}_{(2-x)}\text{O}_4$. All the cases of spectra that produced absorption peaks in the fingerprint region (400 cm^{-1} - 800 cm^{-1}), which is due to M-O stretching

that ensures the presence of ferrites in prepared samples and designates the spinel structure. Stretch vibration bands are associated with the metal are used at the octahedral and tetrahedral bases in this zone. In Table 5 has been shows the spinal structure, the tetrahedral and octahedral sites of spectra values are high-frequency band (ν_1) (560 cm^{-1} - 620 cm^{-1}) and short frequency (ν_2) (420 cm^{-1} - 472 cm^{-1}) [32], respectively. The scale of ν_1 exposes that the tetrahedral combination's shuddering is superior to that of the octahedral bases (ν_2) as resulting in lower bonding strength. The shorter bonding length performance in tetrahedral sites confirms the presence of cadmium ions in the micro-level at the internal structure. However, absorption bands are observed as an expected range for ν_1 , ν_2 , and band position difference has mainly occurred while the influence of Fe^{3+} - O^{2-} in octahedral and tetrahedral sites. Fig6 shows a brand value of nearly 1052 cm^{-1} indicates stretching vibration of the C-O group and 1443.2 cm^{-1} indicates the presence O-H group. The band ranges 3000 cm^{-1} - 1600 cm^{-1} are shows the O-H group and impurities on the surface of spinel ferrites and also the existence of the O-H group. The results show that FTIR absorption spectroscopy permits distinguishing the spinel structure and synthetic substances adsorbed on the outside of the nanoparticle [37].

Table 5. FTIR peaks $\text{Co}_{0.5}\text{Zn}_{0.5}\text{Cd}_x\text{Fe}_{(2-x)}\text{O}_4$.

Concentration	$\nu_1(\text{cm}^{-1})$	$\nu_2(\text{cm}^{-1})$
0.0	620	472
0.1	605	460
0.2	585	448
0.3	577	437
0.4	572	425
0.5	560	420

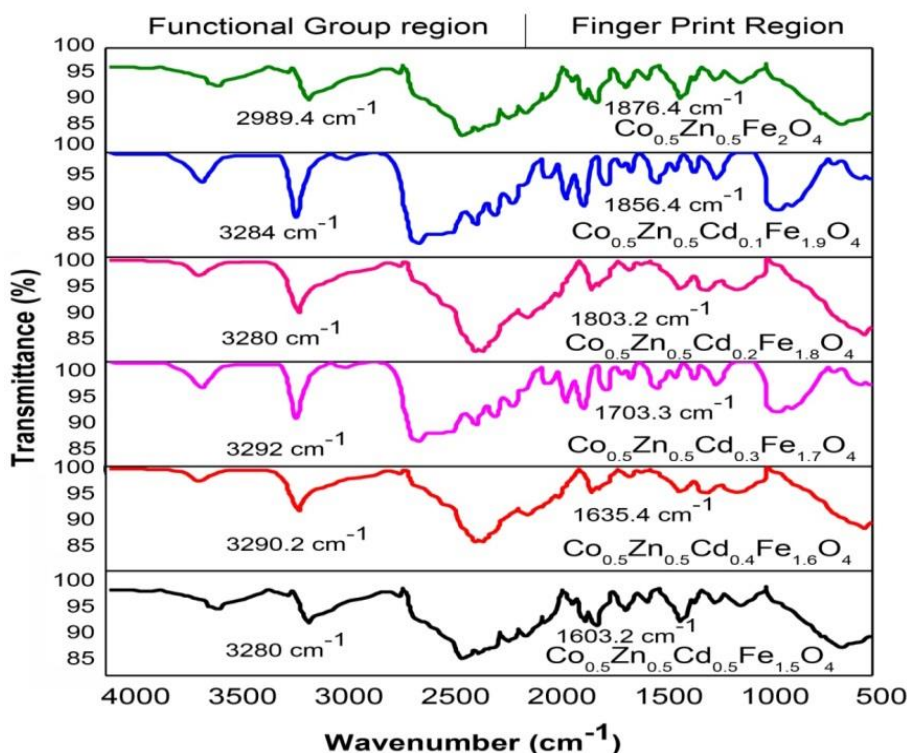


Fig.6. FTIR Spectra of $\text{Co}_{0.5}\text{Zn}_{0.5}\text{Cd}_x\text{Fe}_{(2-x)}\text{O}_4$ ferrites.

4.4. TEM characterization

Fig 7 shows the lattice fringes and particle distribution shape of the nanoparticles on $Co_{0.5}Zn_{0.5}Cd_xFe_{(2-x)}O_4$ ferrofluids. Transmission Electron Microscope (TEM) was performed to analyze the ferrite samples. TEM analysis of images reveals the agglomeration of particles, which may occur due to nano-sized effect, the magnetic interaction between the magnetic nanoparticles, and high annealing temperature as same reported by Upadhyay et al [33]. Agglomeration of nanoparticles is unavoidable because it is completely dependent on high temperatures. The observed TEM image shows the spherical shape of nanoparticles in crystalline nature. This obtained the crystal size range from 28 nm to 35.63 nm for Co-Zn ferrites and Cd and Fe doped samples. The approximately final particle size of the Cobalt is found 25.35 nm and the zinc added nanoparticles size increased to 35.63 nm. This may be due to Zn^{2+} having a zero magnetic moment, which converts the cobalt ions to tetrahedral bases A. Similarly, Cd^{2+} ion-doped models perform the same Zn^{2+} ions as Cd^{2+} ion concentrations increase. With cadmium doping, molecule size expanded more from 28 nm to 35 nm and it is undeniably true that roughly the same scope of molecule size is gotten for every one of the pre-arranged examples by XRD strategy as given in Table 2 for correlation. Fig 7 shows the SAED in inverse transform (IFFT) of a selected region of $Co_{0.5}Zn_{0.5}Cd_xFe_{(2-x)}O_4$ nanoparticles. The inverse Fourier transition from the SAED shape indicates that the planes are preferably in the same direction, thus ensuring the periodicity of the crystal configuration for these spinel ferrites.

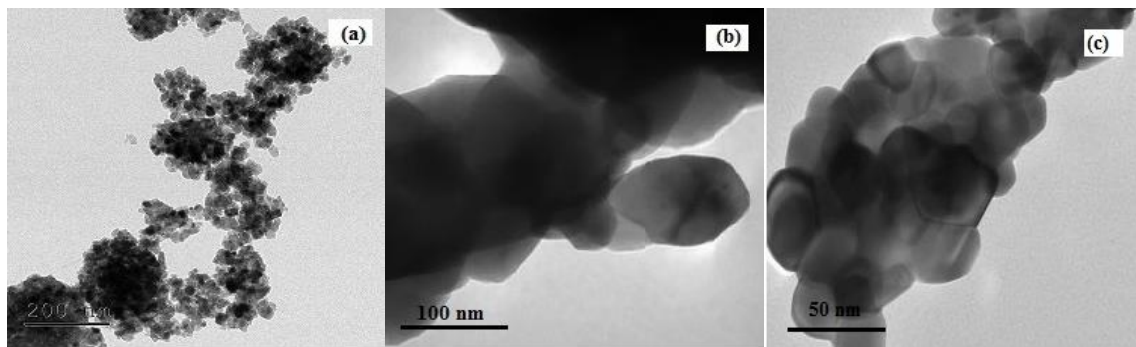


Fig.7. TEM representations of $Co_{0.5}Zn_{0.5}Cd_xFe_{(2-x)}O_4$ ferrites.

Fig 8 shows the HRTEM of $Co_{0.5}Zn_{0.5}Cd_xFe_{(2-x)}O_4$ ferrite sample with two different measurements. The nanoparticles generated by this approach are crystalline materials, as seen in the HRTEM micrograph on a 24.56 nm scale (Fig 8). The foreground in the picture is from the other side, depicts particular nanoparticles selected area interference pattern (SAED) [35].

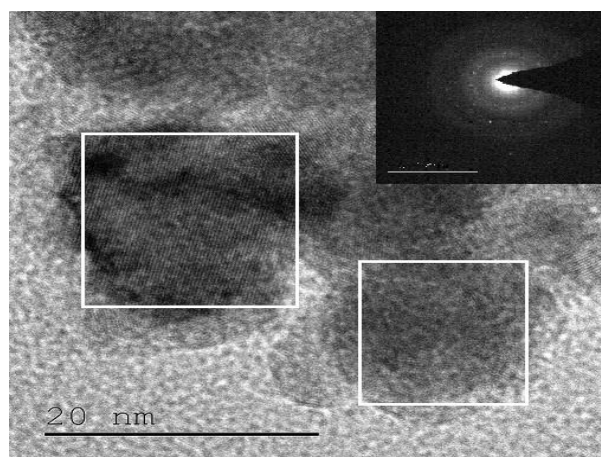


Fig.8. HRTEM of $Co_{0.5}Zn_{0.5}Cd_xFe_{(2-x)}O_4$ ferrite sample with diffraction pattern as selected area.

The image's lattice patterns correlate to a cluster of atomic planes inside these nanoparticles, revealing that they are functionally homogeneous. Conversely, such fringe patterns represent a material with highly crystalline progress of the construction by well-defined diffraction bands. Fig9 shows the histogram of $Co_{0.5}Zn_{0.5}Cd_xFe_{(2-x)}O_4$ ferrites nanoparticles from the TEM studies by using the Gaussian fit method. The particle size and different grid systems of an average number of particles size are close to 40. The symmetric profile was observed from the Gaussian fit at the region 9.0nm for prepared samples. The size of the Cd doped Co-Zn ferrites are good agreed with the estimated crystal size from the X-ray diffraction peak intensities (Scherer's formula). The sizes of the particle were estimated by using software image J as shown in Fig 10.

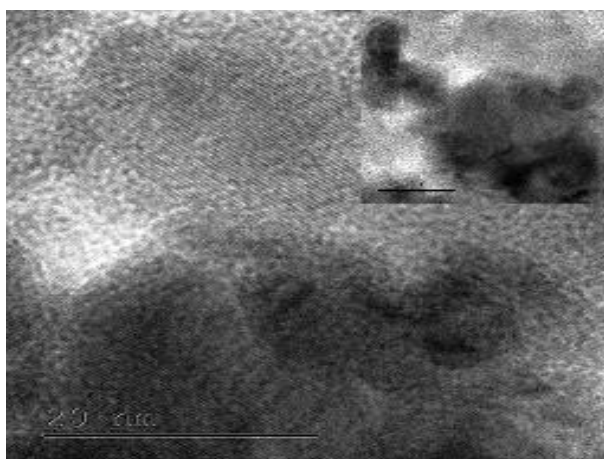


Fig.9. Inverse Fourier transform (IFFT) from TEM.

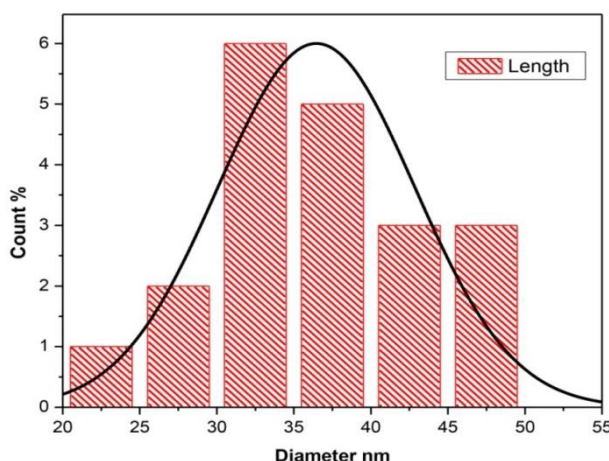


Fig.10. $Co_{0.5}Zn_{0.5}Cd_{0.5}Fe_{1.5}O_4$ Crystallite size is 35.63 nm.

4.5. TG/DTA

TG/DTA analysis was carried out from room temperature at 800⁰ C to identify the thermal decomposition of Co-Zn ferrite samples and recorded data as shown in Fig11. Starting material like iron oxide black-brownish was chosen for $CoFe_2O_4$. The thermal analysis of the TG/DTA curve represents the weight losses by degradation of ferrite nano particles. The DTA bend clarifies the heat needed to expand the temperature of the prepared ferrites and tracked down a negative lower amount of heat around between 850 °C to 1000 °C. In any case, at first, the TG/DTA bend demonstrates weight reduction and its examination affirms about heat deterioration of the cobalt

ferrite nanomaterial being scrutinized. The DG / DTA curve maturity correlation proves to be endothermic in the environment and the arrangement of ferrite ranges from 450^oC to 720^oC observed from the dynamic section.

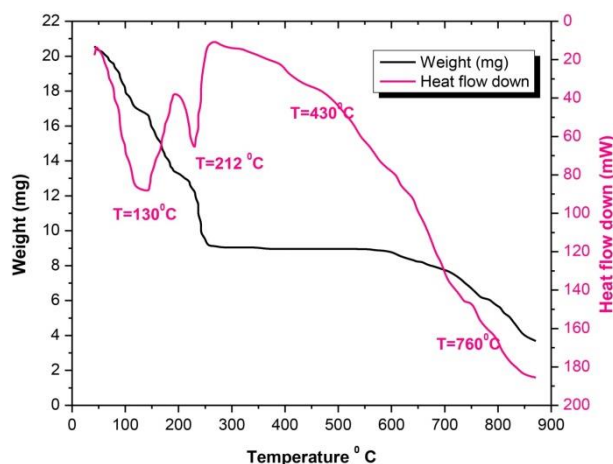


Fig.11.TG/DTA curve for $Co_{0.5}Zn_{0.5}Cd_xFe_{(2-x)}O_4$ ferrites ($x=0.5$).

5. Conclusion

The cadmium doped Co-Zn ferrites $Co_{0.5}Zn_{0.5}Cd_xFe_{(2-x)}O_4$ ($x=0.0, 0.1, 0.2, 0.3, 0.4,$ and 0.5) are synthesized successfully by the co-precipitation method. The TG-DTA curves show the endothermic nature of the ferrite samples synthesis reaction succeeds at 720^oC. FTIR and XRD studies revealed the spinel structure in the Co-Zn ferrofluid nanoparticles. Lattice constant was originated to diminish from 8.442 Å to 8.403 Å with an increment in the centralization of Cd²⁺ particles while crystallite size expanded from 25.35 nm to 35.63 nm with cobalt focus. This may be due to the presence of increasing molecular concentration on the crystal surface which leads to increasing grain growth. The shrinkage was observed from the ferrite samples for $Co_{0.5}Zn_{0.5}Fe_2O_4$ ($x=0.0$). W-H plot method shows the tensile and compressive nature of the material and strain value obtained as 0.0024 -0.0021 for prepared samples. The crystal size is calculated by using Debye Scherer's formula for the prepared samples found to be good agreed with the W-H plot. X-ray density of ferrites observed an increasing trend from 5.185g/cm³ to 5.984 g/cm³ and the porosity diminished with an increase of Cd ion concentrations. The hopping length was found in a decreasing manner for tetrahedral L_A and octahedral L_B sites 3.6707 Å - 3.6332 Å and 2.9967 Å -2.9662 Å respectively. It may be due to the addition of Cd²⁺ ions with smaller radii ions and larger radii ions. FTIR bands show the shift of retention groups towards low wavelength locations with expansion in cadmium concentrations.

With the expansion of cadmium ion concentrations on Co-Zn ferrites observed from the FTIR low wavenumber by shifting the absorption curve. This investigation also discussed dislocations density (ρ_D), Ionic radii (r_A) and (r_B), and stacking fault coefficient (α) of cadmium doped Co-Zn ferrites also reported. Furthermore, TEM analysis revealed the spherical shape of ferrite nanoparticles which ensured that the formations of nanoparticles with high agglomeration were found due to the communications between the magnetic nanoparticles in prepared samples. Those crystal sizes received from TEM studies are good agreed with the experimental and theoretical calculated values.

Acknowledgements

I thank Dr. S. Sendhilnathan, (Associate Professor) for their expertise and assistance throughout all aspects of our study and for their help in writing the manuscript.

References

- [1] V.A. Bharati, Sandeep B. Somvanshi, Ashok V. Humbe, V.D. Murumkar, V.V. Sondur, K.M. Jadhav, *J. Alloys Compd.* 821, 153501(2020); <https://doi.org/10.1016/j.jallcom.2019.153501>
- [2] Sandeep B. Somvanshil, R. Vipin Kumar, Jitendra S. Kounsalye1, Tukaram S. Saraf1, and K. M. Jadhav1., *AIP Conference Proceedings.*, AIP Publishing, 2115, 030522(2019).
- [3] A. Abu El-Fadl, Ragaa S. Mahmoud, A. A. Abu-Sehly, El Sayed Yousef, E. R. Shaaban, Mohamed N. Abd-el Salam, *Journal of Ovonic Research*, 17 (6), 499-507 (2021).
- [4] S.B. Kale, Sandeep B. Somvanshi, *AIP Conference Proceedings*, AIP Publishing LLC1953 (6), 030193 (2018).
- [5] S.B. Somvanshi, Mangesh V Khedkar, K. M. Jadhav, *Ceram. Int.* 46 (7), 8640-8650 (2020); <https://doi.org/10.1016/j.ceramint.2019.12.097>
- [6] J. EL Ghoul, G. A. Khouqeer, *Journal of Ovonic Research*, 16 (5), 273-279 (2020).
- [7] R. Sharma, P. Thakur, M. Kumar, P. Sharma, V. Sharma, *J. Alloy. Compd.* 746(6), 532-539 (2018); <https://doi.org/10.1016/j.jallcom.2018.02.287>
- [8] R. Mondal, S. Dey, K. Sarkar, P. Dasgupta, S. Kumar, *Mater. Res. Bull.* 102(4), 160-171 (2018); <https://doi.org/10.1016/j.materresbull.2018.02.016>
- [9] D. B. Basha, D. Dahiya, E. *Journal of Ovonic Research*, 17 (6), 589-594 (2021).
- [10] M. Rahimi, Parviz Kameli, Mehdi Ranjbar, Hadi Salamati, *J. Magn. Magn Mater.* 347(18), 139-145 (2013); <https://doi.org/10.1016/j.jmmm.2013.08.004>
- [11] N. Amin, M. I. Arshad, M. Ajaz-un-Nabi, K. Mahmood, M. Z. Iqbal, A. Ali, M. T. Wahla, M. Sharif, M. Asif, N. Sabar, S. Ikram, M. R. Ahmad, Z. Farooq, K. Hussain, A. Bibi, G. Mustafa, *Journal of Ovonic Research*, 15 (1), 27-35 (209).
- [12] A.V.Raut, ,D.R.Shengule, K.M.Jadhav, *J. Magn. Magn Mater.* 358 (12); 87-92(2014); <https://doi.org/10.1016/j.jmmm.2014.01.039>
- [13] P. Coppola, F. G. da Silva, G. Gomide, F. L. O. Paula, A. F. C. Campos, R. Perzynski, C. Kern, J. Depeyrot & R. Aquino, *J. Nanoparticle Res.* 18 (5) ,138 (2016); <https://doi.org/10.1007/s11051-016-3430-1>
- [14] G. Pratibha, A. Thirupathi, V. K. Vamsi Krishna, P. Siva Kumar, G. K Siva Sankara Yadav, *Journal of Ovonic Research*, 17 (4), 323-331 (2021).
- [15] R. Topkaya, A. Baykal, A. Demir, *J. Nanoparticle Res.* 15 (1); 1359 (2013); <https://doi.org/10.1007/s11051-012-1359-6>
- [16] Hojat Khedri & Ahmad Gholizadeh, *Applied Physics A*, 125 (3), 709 (2019).
- [17] S. Dey, R. Mondal, S.K. Dey, S. Majumder, P. Dasgupta, A. Poddar, V.R. Reddy, S. Kumar, *J. Appl. Phys.* 118 (6), 103905 (2015); <https://doi.org/10.1063/1.4930801>
- [18] R. Mondal, S. Dey, K. Sarkar, P. Dasgupta, S. Kumar, *Mater. Res. Bull.* 102(5), 160-171(2018); <https://doi.org/10.1016/j.materresbull.2018.02.016>
- [19] T.R. Tatarchuk, N.D. Paliychuk, M. Bououdina, B. Al-Najar, M. Pacia, W. Macyk, A. Shyichuk, *J. Alloy. Compd.* 731(2), 1256-1266(2018); <https://doi.org/10.1016/j.jallcom.2017.10.103>
- [20] I. Sharifi, H. Shokrollahi, *J. Magn. Magn. Mater.* 324(15), 2397-2403(2012); <https://doi.org/10.1016/j.jmmm.2012.03.008>
- [21] G. Barrera, M. Coisson, F. Celegato, S. Raghuvanshi, F. Mazaleyrat, S.N. Kane, P. Tiberto, *J. Magn. Magn. Mater.* 456 (1), 372-380 (2018); <https://doi.org/10.1016/j.jmmm.2018.02.072>
- [22] R. J. Ramalingam, P. K. Nayak, A. J. Nelson, T. Radhika, H. A. AL-Lohedan, Z. A. Issa *Journal of Ovonic Research*, 16 (6), 361-367 (2020).
- [23] X. Huang, J. Zhang, W. Wang, T. Sang, B. Song, H. Zhu, W. Rao, C., *J. Magn. Magn. Mater.* 405(1), 36-41(2016); <https://doi.org/10.1016/j.jmmm.2015.12.051>
- [24] T.R. Tatarchuk, M. Bououdina, N.D. Paliychuk, I.P. Yaremiy, V.V. Moklyak, *J. Alloy. Compd.* 694 (8), 777-791; <https://doi.org/10.1016/j.jallcom.2016.10.067>
- [25] S. Dey, S.K. Dey, B. Ghosh, P. Dasgupta, A. Poddar, V.R. Reddy, S. Kumar *J. Appl.*

- Phys,114(4), 093901 (2013); <https://doi.org/10.1063/1.4819809>
- [26] K. S. Rathore, Deepika D. Patidar, N. N. Saxena, K. B. Saxena, Journal of Ovonic Research, 5 (6), 175-185 (2009).
- [27] S. Dey, S.K. Dey, K. Bagani, S. Majumder, A. Roychowdhury, S. Banerjee, V.R. Reddy, D. Das, S. Kumar, Appl. Phys. Lett. 105 (6), 063110 (2014); <https://doi.org/10.1063/1.4893028>
- [28] F. Tourinho, R. Franck, R. Massart, Journal of Materials Science 25 (7), 3249-3254 (1990); <https://doi.org/10.1007/BF00587682>
- [29] J. Chen, Y. Wang, Y. Deng, J. Alloys Compd. 552 (5), 65-69 (2013); <https://doi.org/10.1016/j.jallcom.2012.10.073>
- [30] S. Anwar, J. Ahmad, T. Zia, H. Kimura, K. B. Saxena, Journal of Ovonic Research, 12 (1), 35-41 (2016).
- [31] A.T. Pathan, S.N. Mathad, A.M. Shaikh, Int. J. Self Propag. High Temp. Synth. 23 (2), 112-117 (2014); <https://doi.org/10.3103/S1061386214020083>
- [32] M.K. Rendale, S.N. Mathad, V. Puri, Micro electron. Int.34 (2) ,57-63(2017); <https://doi.org/10.1108/MI-02-2016-0009>
- [33] Meenal Gupta, Anusree Das, Satyabrata Mohapatra, Dipankar Das & Anindya Datta, Applied Physics A, 126(6), 660(2020); <https://doi.org/10.1007/s00339-020-03823-9>
- [34] C. Upadhyay, H.C. Verma, S. Anand, J. Appl. Phys. 95(4), 5746-5751(2005); <https://doi.org/10.1063/1.1699501>
- [35] M. T. Farid, I. Ahmad, S. Aman, M. Kanwal, G. Murtaza, I. Ali, I. Ahmad, M. Ishfaq, Journal of Ovonic Research, 11 (1), 1-10 (2015).
- [36] Kaur, H., Singh, A., Kumar, V., & Ahlawat, D. S, Journal of Magnetism and Magnetic Materials.474(8), 505-511(2019); <https://doi.org/10.1016/j.jmmm.2018.11.010>
- [37] E. M. M. Ibrahim, A. Z. Mahmoud, L. Galal, Y. El Sayed, E. R. Shaaban, Journal of Ovonic Research, 17(6), 519-532 (2021).